ACS APPLIED MATERIALS & INTERFACES

Research Article

www.acsami.org

Fabrication of Single Cylindrical Au-Coated Nanopores with Non-Homogeneous Fixed Charge Distribution Exhibiting High Current Rectifications

Saima Nasir,[†,‡] Mubarak Ali,*[,†,‡] Patricio Ramirez,[§] Vicente Gómez,[§] Bernd Oschmann,[⊥,∥] Falk Muench,[†] Muhammad Nawaz Tahir,[#] Rudolf Zentel,[⊥] Salvador Mafe,[⊗] and Wolfgang Ensinger[†]

[†]Department of Material- and Geo-Sciences, Materials Analysis, Technische Universität Darmstadt, D-64287 Darmstadt, Germany

[‡]Materials Science Department, GSI Helmholtzzentrum für Schwerionenforschung, D-64291, Darmstadt, Germany

[§]Departament de Física Aplicada, Universitat Politècnica de València, E-46022 València, Spain

[⊥]Institut für Organische Chemie and [#]Institut für Anorganische Chemie und Analytische Chemie, Johannes Gutenberg-Universität, D-55099 Mainz, Germany

[∥]Graduate School Materials Science in Mainz, Staudinger Weg 9, D-55128, Mainz, Germany

[⊗]Departament de Física de la Terra i Termodinàmica, Universitat de València, E-46100 Burjassot, Spain

ABSTRACT: We designed and characterized a cylindrical nanopore that exhibits high electrochemical current rectification ratios at low and intermediate electrolyte concentrations. For this purpose, the track-etched single cylindrical nanopore in polymer membrane was coated with a gold (Au) layer via electroless plating technique. Then, a non-homogeneous fixed charge distribution inside the Au-coated nanopore was obtained by incorporating thiol-terminated uncharged poly(*N*-isopropylacrylamide) chains in series to poly(4-vinylpyridine) chains, which were positively charged at acidic pH values. The functionalization reaction was checked by measuring the current−voltage curves prior to and after the chemisorption of polymer chains. The experimental nanopore characterization included the effects of temperature, adsorption of chloride ions, electrolyte concentration, and pH of the external solutions. The results obtained are further explained in terms of a theoretical continuous model. The combination of well-established chemical procedures (thiol and self-assembled monolayer formation chemistry, electroless plating, ion track etching) and physical models (two-region pore and Nernst−Planck equations) permits the obtainment of a new nanopore with high current rectification ratios. The single pore could be scaled up to multipore membranes of potential interest for pH sensing and chemical actuators.

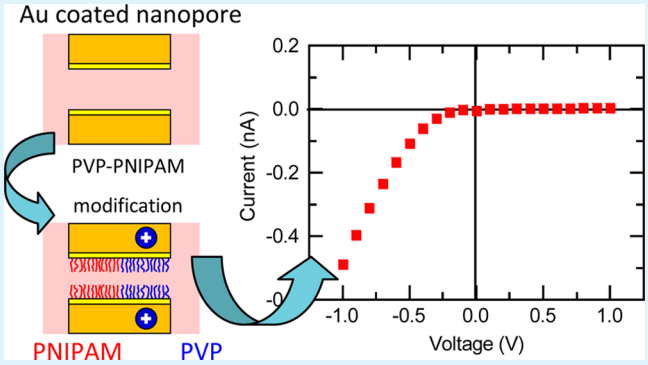

KEYWORDS: *synthetic nanopores, chemical functionalization, stimuli-responsive polymers, current rectification, electroless gold plating, Nernst−Planck equations*

1. INTRODUCTION

Ion current rectification (ICR) is involved in most applications of synthetic nanopores,[1,2] nanochannels,[3] nanoelectrodes,[4] film interfaces[5] and nanopipettes[6,7] concerning nanofluidic circuits,[3,8−15] ratchet effects,[16−18] energy harvesting,[19,20] molecular separation,[21] drug delivery,[22] and biochemical sensing.[23−30] ICR is observed as a diode-like current−voltage (I−V) characteristic, with high and low conducting states depending on the polarity of the applied voltage that reveal preferential directions for ion transport.[2,6]

It has been theoretically and experimentally demonstrated that the interactions of mobile ions with the active charged groups fixed at the pore surface are responsible for the asymmetrical conductance.[31−35] ICR can be achieved using either pores with asymmetric shapes or pores with non-homogeneous fixed charge distributions. The heavy ion track-etch technology has already reached commercialization. Therefore, devices based on this technique can be fabricated using polymeric membranes containing nanometric single pores with a variety of shapes and charged groups, which are sensitive to different external stimuli.[2,8,13,14,21,33,36−41] Rectification ratios r are defined as the absolute value of the quotient between the electric current in the high and low conducting states at a given voltage. As-prepared track-etched conical nanopores with carboxylic groups homogeneously distributed on the pore surface show $r \approx 7$ at electrolyte concentration $c \approx 0.1$ M KCl and applied voltage $V \approx 1$ V.[31,42]

Received: April 21, 2014
Accepted: July 22, 2014
Published: July 22, 2014

These values can be enhanced up to $r \approx 20$ using asymmetric pores with bulletlike tips[43,44] under the same conditions. Symmetric pores with non-homogeneous fixed charge distributions display also rectification ratios of the same order of magnitude.[2,38,45,46] Recently, cylindrical nanopores showing rectification induced by nanoparticle blocking and release have also been reported.[47] A significant improvement can be obtained using conical or double conical pores in polymeric membranes with bipolar charge density distributions[33,40] or asymmetrical pores externally tunable by voltage gating,[9,48] where rectification ratios of the order of several hundreds can be achieved.

In this paper, we report a nanopore showing high rectification ratios ($r \approx 100$) at low and intermediate electrolyte concentrations. It consists of a cylindrical Au-coated nanopore where ICR is achieved by means of a non-homogeneous fixed charge distribution with neutral poly(*N*-isopropylacrylamide) (PNIPAM) chains decorating one-half of the pore and poly(4-vinylpyridine) (PVP) molecules, which are positively charged at acidic pH values, covering the other pore half. We present a complete experimental characterization of the pore rectification and discuss the results in terms of a theoretical model accounting for ion transport through the nanopore.[31]

2. EXPERIMENTAL SECTION

2.1. Materials. All the reagents used in the experimental work are of analytical grade and were used as received without further purification: sodium hydroxide (Carl Roth, 99%, p.a.), ethanol (Sigma-Aldrich, anhydrous), 4-(dimethylamino)pyridine (Fluka, puriss.), $AgNO_3$ (Grüssing, p.a.), ethanol (Brenntag, 99.5%), formaldehyde solution 36.5% stabilized with methanol (Fluka, puriss. p.a.), methanol (Aldrich, 99.8%), Na_2SO_3 (Merck, p.a.), $(NH_4)_3[Au(SO_3)_2]$ solution (Galvano gold bath from Schütz Dental GmbH, 15 g of gold 99.9% per liter), NH_3 33% in water (Merck, puriss.), $SnCl_2$ dihydrate (Sigma-Aldrich, ACS reagent), and trifluoroacetic acid (Riedel-de Häen, >99%). Thiol-terminated PVP [P8383−4VPSH, Mn = 2.5,000] was purchased from Polymer Source, Inc.

For the synthesis of thiol-terminated PNIPAM, monomer *N*-isopropylacrylamide (NIPAM) was purchased from Acros Organics and was recrystallized from hexane. α,α'-Azoisobutyronitrile (AIBN, Sigma-Aldrich) was recrystallized from diethyl ether. All solvents were purchased from Sigma-Aldrich and dried before use.

Polyethylene terephthalate (PET) membranes (Hostaphan RN 12, Hoechst) of 12 μm thickness were irradiated at the GSI Helmholtz Centre for Heavy Ion Research (Darmstadt) with single swift heavy ions (gold ions of kinetic energy of 11 MeV per nucleon). Subsequently, ion-tracked PET membranes were further exposed to soft UV light from each side for 15 min to sensitize the latent tracks for the etching process. The UV lamp used for irradiation of PET membranes was homemade and equipped with T-30 M UV-B fluorescent tubes purchased from Vilber-Lourmat, Germany. The power consumption of the tube is 30 W and gives UV−B light of wavelength 312 nm (280−380 nm).

2.2. Fabrication of Cylindrical Nanopores. The cylindrical nanopores in polymer membranes were fabricated through symmetric track-etching technique in which the etchant can attack and dissolve the latent ion tracks in polymer membrane from both sides. The etching of latent ion track was carried out in a double-walled isothermal bath at 50 °C, which was half-filled with aqueous 2 M sodium hydroxide (NaOH) solution. The temperature of etching solution was maintained at 50 °C by a circuit of water flowing through the double walls of the beaker. The sensitized ion-tracked polymer membranes were first fixed in the sample holders. Then this sample holder with membranes was immersed in the preheated etching bath. The etching of the samples was carried out for preset time according to the required pore diameter. Moreover, the concentration of the solution and the temperature in the vicinity of the ion-tracked polymer membranes were kept approximately constant throughout the whole etching process because of constant stirring of the etchant. After the etching, the sample holders along with etched polymer membranes were taken out from the etching bath and rinsed several times with deionized water.

2.3. Electroless Plating of Track-Etched Nanopores. Prior to electroless plating, silver nanoparticle seeds were introduced by immersion of the PET membrane having a single cylindrical pore in a sensitization solution (42 mM $SnCl_2$ and 71 mM trifluoroacetic acid in methanol/water = 1:1), followed by washing with ethanol and application of an activation solution (59 mM $AgNO_3$ and 230 mM NH_3 in water).[49] Sn(II) adsorbed onto the membrane surface reduces the Ag(I) in the activation solution, leading to the precipitation of Ag nanoparticles. During this reaction, the initially colorless membranes turned slightly brownish. After activation, the PET membrane was covered with gold using an electroless plating bath optimized for the deposition of homogeneous, thin nanoscale films.[50] Briefly, the plating bath consisted of formaldehyde (reducing agent), sulfite (excess ligand), disulfitoaurate (gold source), and 4-(dimethylamino)pyridine (auxiliary reagent). Gold nanofilm deposition was indicated by a shift of the membrane color to dark blue.

2.4. Synthesis of Thiol-Terminated PNIPAM. *S*-1-Dodecyl-*S*-(α,α'-dimethyl-α''-acetic acid)trithiocarbonate (DMP) was synthesized following the previously reported procedure.[51] For the reversible, addition−fragmentation chain transfer (RAFT) polymerization, *N*-isopropylacrylamide (1.50 g, 13 mmol), DMP (48.3 mg, 0.13 mmol) as a chain-transfer agent (CTA), azoisobutyronitrile (2.2 mg, 0.013 mmol) as an initiator, and 2 mL of dioxane were added to a Schlenk tube following a previously described method.[52] The oxygen was exchanged by nitrogen by applying three freeze−pump−thaw cycles. The mixture was then stirred in an oil bath at 70 °C overnight. The reaction mixture was precipitated three times in hexane/tetrahydrofuran (THF) mixture and dried under reduced pressure to yield a yellow powder as PNIPAM-CTA.

PNIPAM-CTA: Yield: 48% as yellow powder; molecular weight: M_n(NMR) = 5900 g mol^{-1}, M_n(GPC) = 5300 g mol^{-1}, polydispersity index (GPC) = 1.22; UV−vis: absorption at 310 nm.

The thiol-terminated PNIPAM (PNIPAM-SH) was obtained by aminolysis of the trithiocarbonate end group of the PNIPAM-CTA with hexylamine in the presence of tributylphosphine in a molar ratio of 1:5:1. The reaction was performed in THF, whereas the reaction mixture was stirred for 3 h at room temperature. The color of the reaction mixture turned from yellow to colorless indicating the successful reaction, which was also confirmed by UV−vis spectroscopy, where a complete loss of the absorption at 310 nm was observed.

PNIPAM-CTA: Yield: 93% as colorless powder; molecular weight: M_n(GPC) = 6150 g mol^{-1}, PDI(GPC) = 1.23; UV−vis: no absorption at 310 nm.

2.5. Functionalization of Au-Coated Nanopores. The chemisorption of polymer chains on the single Au nanotube was achieved via thiol chemistry. For this purpose, solutions of thiol-terminated PNIPAM-SH (3 mg/mL) and thiol-terminated PVP-SH (3 mg/mL) were prepared in anhydrous ethanol, separately. Then, the polymer membrane with the single Au nanotube was fixed between the two chambers of a conductivity cell. The right compartment was filled with a solution of PVP-SH, while the left one contained the PNIPAM-SH solution. The chemisorption was carried out for 20 h at room temperature. Then the functionalized Au-coated pore was washed several times with ethanol followed by deionized water for the removal of physically adsorbed polymer molecules. Figure 1 shows a simplified scheme for the functionalization of the single cylindrical Au-coated nanopore.

2.6. Measurement of Current−Voltage (*I*−*V*) Curves. The single Au-coated pore membrane (unmodified and modified) is characterized by measuring the *I*−*V* curves. To this end, the membrane is clamped between the two halves of an electrochemical conductivity cell. The electrolyte (0.1 M KCl) solution was prepared in a phosphate buffer (10 mM, pH = 7.5). The pH of the acidic solution, pH = 2.8, is adjusted with dilute HCl. The corresponding electrolyte solution was filled on both sides of the membrane. An Ag/AgCl standard reference electrode was placed into each half-cell solution, and the ionic current flowing across the membrane was measured with a picoammeter/voltage source (Keithley 6487, Keithley Instruments, Cleveland, OH).

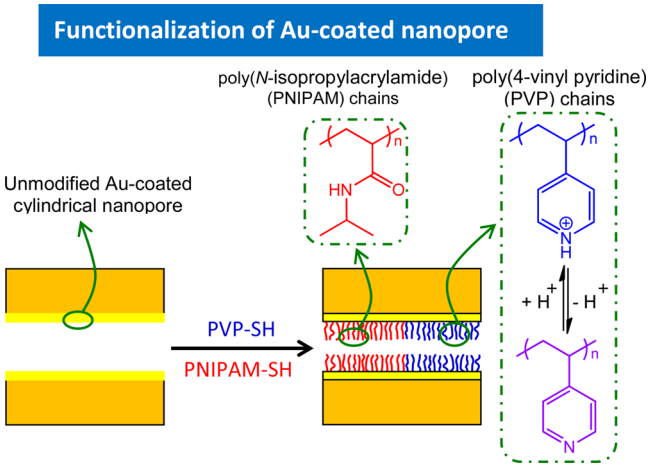

Figure 1. Simplified scheme for the functionalization of a single cylindrical Au-coated nanopore and the charged states of poly(4-vinylpyridine) chains at different pH conditions.

$I-V$ curves were recorded by applying a scanning triangle voltage signal from −2 to +2 V across the membrane.

3. THEORETICAL MODEL

The steady-state ionic transport through the nanopores has been analyzed theoretically in terms of a continuous model based on the Poisson−Nernst−Planck (PNP) equations.[31]

$$\nabla^2\phi = -\frac{F}{\varepsilon}\sum_i z_i c_i \tag{1}$$

$$\nabla\cdot\vec{J}_i = -\nabla\cdot\left[D_i\left(\nabla c_i + z_i c_i \frac{F}{RT}\nabla\phi\right)\right] = 0 \tag{2}$$

where z_i, $c_i(x)$, D_i, and $\vec{J}_i$ are, respectively, the charge number, local concentration, diffusion coefficient, and flux density of ion i, respectively. The F and R terms are the Faraday and universal gas constants, T is the absolute temperature, $\phi(x)$ is the local electric potential, and ε is the electrical permittivity. Numerical integration of eqs 1 and 2 gives the ionic flux densities, the total electric current I, and the profiles of ionic concentrations and electric potential through the nanopore at an applied voltage V and fixed external concentrations. The ground electrode is placed on the left solution, and positive currents flow from the right to the left solution as shown in Figure 2. It has been assumed that the external solutions are ideal and perfectly stirred and that the whole system is isothermal and in steady-state. In eq 2, the contribution from the electro-osmotic flow (EOF) was ignored as a first approximation. Although this contribution can be noticeable in certain cases,[53,54] recent studies have demonstrated that EOF can be ignored in synthetic pores analogous to those studied here.[55,56] Indeed, simple order of magnitude estimations reveal that the EOF can be safely ignored in our experiments and do not seem to be responsible for the high rectification ratios observed here. Moreover, increased viscosity effects caused by the brush chains occluding a significant

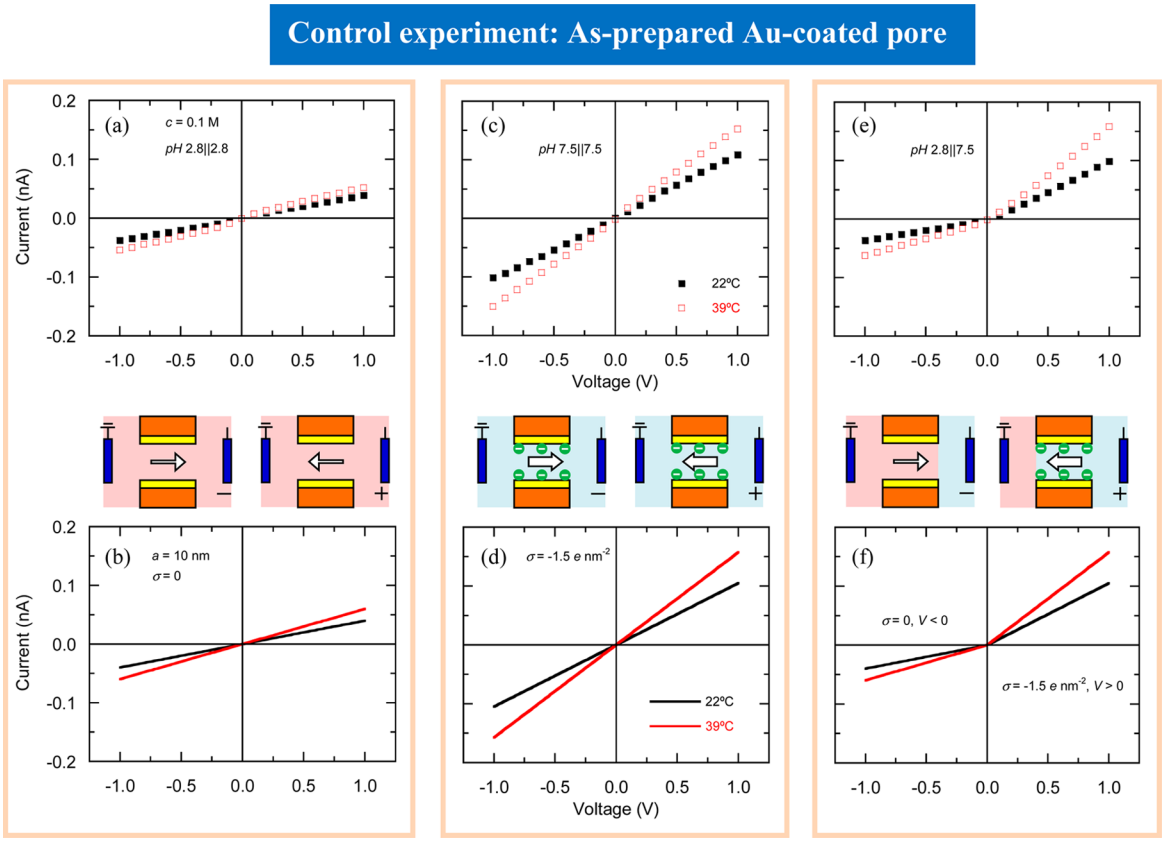

Figure 2. Experimental and theoretical $I-V$ curves for the as-prepared Au-coated cylindrical pore. The cartoons describe the different experimental conditions considered. (a) Experiments and (b) theoretical results for the pH configuration 2.8||2.8. (c) Experiments and (d) theoretical results for pH 7.5||7.5. (e) Experiments and (f) theoretical results for pH 2.8||7.5. The curves are parametric in the temperature.

dx.doi.org/10.1021/am502419j | ACS Appl. Mater. Interfaces 2014, 6, 12486−12494

part of the pore can decrease even further the water convective movement through the pore.

The theoretical model considered is simple, but it can explain most of the experimental results found, as we will show later. Furthermore, the PNP model used has become the standard theoretical formalism in the field and has been applied previously to describe the ionic transport in pores with a variety of shapes and fixed charge distributions;[3,32−34,40,56] further details about the numerical procedure used here can be found elsewhere.[31]

4. RESULTS AND DISCUSSION

To homogeneously cover the ion-track etched membrane with a thin gold film, an electroless plating reaction optimized for nanomaterial fabrication was applied. As shown before,[50] this reaction leads to a highly surface-conformal deposition of small gold nanoparticles even on complex shaped substrates with extended inner surfaces, as required in the present case.

Figure 2 shows the experimental and theoretical $I-V$ curves for the as-prepared Au-coated cylindrical pore at the indicated $pH_L \| pH_R$ configurations and temperatures. The electrolyte concentration is c = 0.1 M KCl. The experiments at the pH configuration of 2.8||2.8 (Figure 2a) allow for the estimation of the pore radius a. We assume that the Cl^- ions do not adsorb on the Au pore walls at this pH value.[57] Figure 2b shows the calculated curves using a = 10 nm and the surface fixed charge density $\sigma = 0\ e/nm^2$ in the theoretical model. To account for the effects of temperature, we included the electrolyte conductivity increase in the interval of 22−39 °C, assuming in the calculations a 1.5-fold increase in the diffusion coefficients of the ionic species over this temperature interval.[58]

Figure 2c shows the experimental results for the case of pH 7.5||7.5. The currents are higher than those of Figure 2a because of the adsorption of Cl^- ions on the Au pore walls.[57] The linear characteristics of the $I-V$ curve indicate that the adsorption of Cl^- is homogeneous throughout the nanopore. Since the pore radius was determined in the previous experiment, the only free parameter in the theoretical model is the surface charge concentration. Figure 2d shows the calculated $I-V$ curves using a = 10 nm and $\sigma = -1.5\ e/nm^2$, which is within the range of the values found in multipore membranes.[59] The calculations reproduce the experimental trends including again the increase of the solution conductivity in the interval of 22−39 °C. The experimental results for pH 2.8||7.5 (Figure 2e) show rectification now, with high and low conducting states at $V > 0$ and $V < 0$, respectively.

A close inspection of the curves reveals that for $V > 0$, the results of Figure 2e are very similar to those of the case pH 7.5||7.5 in Figure 2c. For $V < 0$, the experimental points of Figure 2e resemble those of pH 2.8||2.8 in Figure 2a. This result can be explained as follows. For $V > 0$, the applied electric field prevents the entrance of H^+ ions from the left solution into the pore (Figure 2e). The pH of the inner pore solution is approximately neutral, the Cl^- ions adsorb on the Au pore wall, and the pore shows currents close to the case of pH 7.5||7.5 in Figure 2c. For $V < 0$, the external electric field drives the H^+ ions into the pore. The pH of the inner solution becomes acidic, the Cl^- ions do not adsorb onto the Au wall, and then the pore behaves as in the case of pH 2.8||2.8 of Figure 2a. Figure 2f shows the theoretical predictions considering this assumption. The good agreement between the experiments and the calculations (Figures 2b,d,f) gives strong support to our assumptions. Since the $I-V$ curves are measured using a triangle wave with alternating $V > 0$ and $V < 0$ half periods,[16] the adsorption−desorption processes of Cl^- ions on the pore walls are reversible. We conclude also that the application of a pH gradient between the two solutions separated by the nanopore does not lead to the formation of a gradual hydrogen concentration change across the inner pore solution. On the contrary, the results suggest that the H^+ ions enter or leave the pore solution depending on the polarity of the applied voltage.

Figures 3−7 show the results obtained for the Au-PNIPAM-PVP modified pore. The PNIPAM and PVP chains decorate the

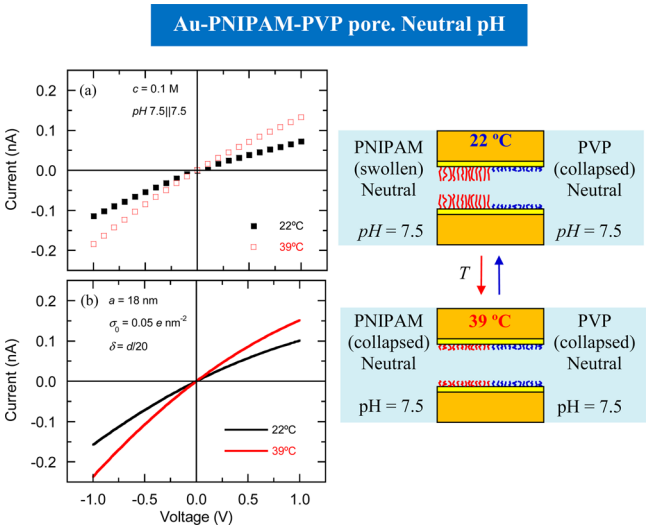

Figure 3. Experimental (a) and calculated (b) $I-V$ curves of the Au-PNIPAM-PVP modified nanopore for the pH configuration of 7.5||7.5. The curves are parametric in the temperature.

left and right sides of the pore, respectively, as indicated in the cartoons describing the different pore configurations. As mentioned above, the PVP chains are in a swollen, positively charged state at acidic pH and in a collapsed, neutral state at pH values around the neutral value. The PNIPAM brushes exhibit a swollen state at 23 °C, and a collapsed state at 39 °C, remaining uncharged at all pH and temperature values. Therefore, the pore displays a nonuniform fixed charge distribution, with a neutral region on the left side and a neutral or positively charged right region, depending on the pH value of the inner solution. To describe this charge distribution, we have assumed that the surface charge density varies with the axial coordinate x following a smooth step function:[32]

$$\sigma(x) = \frac{\sigma_0}{1 + \exp[-2k(x - x_0)]} \tag{3}$$

Parameter k is defined as

$$k = -\frac{1}{\delta} \log\left[\tanh\left(\frac{1}{2}\right)\right] \tag{4}$$

where δ is a characteristic length describing the step thickness. Equation 3 gives $\sigma \approx 0$ for $x \ll x_0$ and $\sigma \approx \sigma_0$ for $x \gg x_0$. This surface charge density is directly related to the volume concentration X of fixed charges in the soft brushes according to[31]

$$X = \frac{2\sigma}{Fa} \tag{5}$$

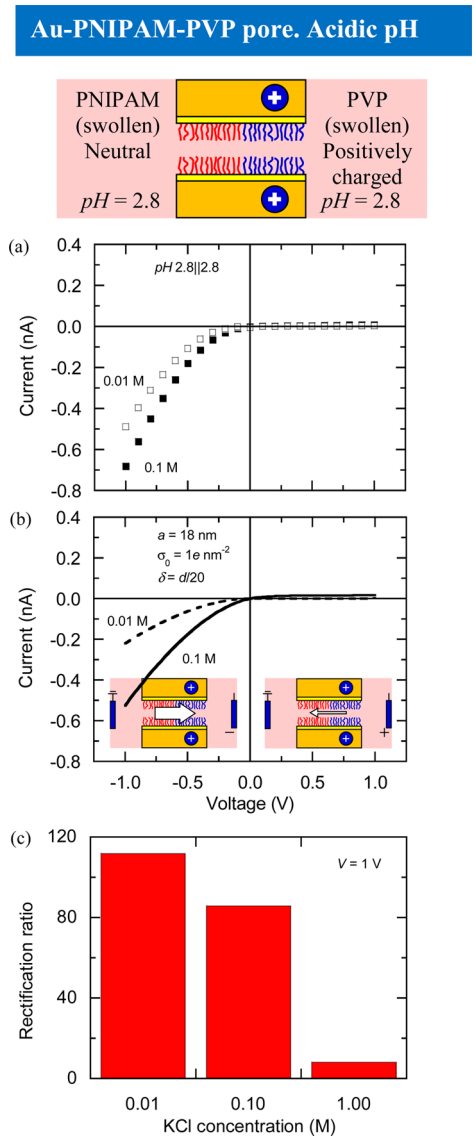

Figure 4. Experimental (a) and calculated (b) $I-V$ curves of the Au-PNIPAM-PVP modified nanopore for the pH configuration of 2.8||2.8. The curves are parametric in the electrolyte concentration. (c) Experimental values of the rectification ratio at $V = 1$ V vs electrolyte concentration.

This equation incorporates the effect of the fixed charges in the polymer brushes and can be used in the PNP framework provided that the convective flow is ignored.

Figure 3 shows the $I-V$ curves of the Au-PNIPAM-PVP modified pore at pH 7.5||7.5. The experimental curves of Figure 3a show a small current rectification, with high and low conducting states at $V < 0$ and $V > 0$, respectively, contrary to the case of the as-prepared (unmodified) Au pore at pH 2.8||7.5 (Figure 2e). This fact suggests that, after modification, the right side of the pore displays a residual positive charge. It can be concluded also that the PNIPAM and PVP chains cover a significant part of the inner surface of the pore, preventing thus the adsorption of Cl^- ions on the Au walls. The theoretical curves of Figure 3b were calculated using $\sigma_0 = 0.05\ e/nm^2$, $x_0 = d/2$ (d is the pore length), $\delta = d/20$, and $a = 18$ nm in the theoretical model (note that the sample used in Figures 3–7 was different from that of Figure 2). The effects of temperature were taken into account assuming again a 1.5-fold increase in the diffusion coefficients of the ionic species over the interval of 22–39 °C.

It has been reported before that conical pores modified with PNIPAM brushes show noticeable increases of the conductance and the ICR with temperature because of the increase in the effective pore diameter that results from the conformational transition of the PNIPAM brushes into a more compact state.[60,61] However, the theoretical results of Figure 3b reproduce the experimental trends without invoking any temperature effect on the left part of the pore other than the increase of the specific electrolyte conductivity. This result is because the present pore radius (18 nm) is significantly higher than the tip radii of the conical pores previously reported (4–7 nm).[60,61] Therefore, the effects of temperature on the PNIPAM chains are small for the pores studied here, and further measurements at 39 °C will not be presented.

Figure 4 shows the results obtained with the Au-PNIPAM-PVP modified pore at pH 2.8||2.8. The experimental $I-V$ curves (Figure 4a) are parametric in the electrolyte concentration. At this pH configuration, all the PVP chains in the right part of the pore are positively charged. The pore displays a high resistance for $V > 0$, when the electric current enters the positively charged end, and a lower resistance for $V < 0$, when the current enters the neutral end (see insets). As expected, the electric current increases with the electrolyte concentration at a fixed voltage because of the increase in the mobile carriers of the solution inside the pore. Figure 4b shows the calculated curves for $\sigma_0 = 1\ e/nm^2$, $x_0 = d/2$, $\delta = d/20$, and $a = 18$ nm. The theoretical results follow qualitatively the experimental data, and the agreement could be improved further by changing slightly the values of x_0 and δ, but these model parameters are not experimentally accessible. The high rectification ratios observed (Figure 4c) constitute the most interesting feature of this pH configuration. The cylindrical, approximately symmetric pore (see Figure 2a) presented here displays high rectification ratios while maintaining a high ionic selectivity because of its relatively small radius.

The PNP model can explain also the high current rectification ratios observed. The pore region decorated with neutral PNIPAM behaves as a diffusion boundary layer (DBL) juxtaposed in series with the positively charged pore region containing the PVP chains. For negative voltages (Figure 5a,b), the mobile carriers accumulate at the PNIPAM||PVP interface (Figure 5a), and most of the applied voltage falls in the bulk of the entire pore. The mobile carrier concentration increases with the negative voltage and, as a result, the current increases rapidly for these voltages. For positive voltages (Figure 5c,d), the PNIPAM||PVP interface becomes depleted of mobile carriers (Figure 5c), the pore resistance increases, and the current attains a limiting value. In this case, most of the applied potential drops at the PNIPAM||PVP interface (Figure 5d). The limiting current attained increases with the electrolyte concentration, and the rectification ratio decreases accordingly, as shown in Figure 4c.

Figure 6 shows the results obtained with the pH configuration of 2.8||7.5. In this case, the PVP chains in contact with the neutral solution are expected to be in a collapsed, neutral state. However, the experimental $I-V$ curve (Figure 6a) shows still rectification, with a high conduction state analogue to that of the case pH 2.8||2.8 for $V < 0$, and a low conduction state for $V > 0$, with currents close to those of the case pH 7.5||7.5. This curve can be explained using similar arguments as in the case of the as-prepared Au nanopore (Figure 2e), assuming that for $V < 0$ protons can diffuse from the left solution and reach the PVP region, giving rise to a positively charged region at the right side

dx.doi.org/10.1021/am502419j | ACS Appl. Mater. Interfaces 2014, 6, 12486–12494

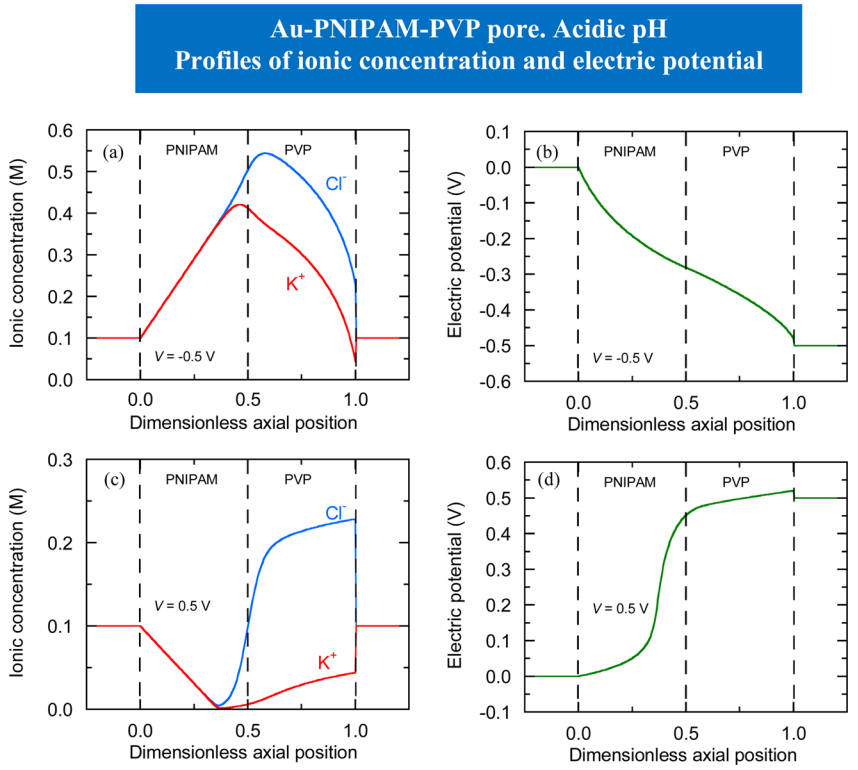

Figure 5. Calculated profiles of ionic concentration (a) and electric potential (b) under negative applied voltages. Calculated profiles of ionic concentration (c) and electric potential (d) under positive applied voltages. The results correspond to the pH configuration of 2.8||2.8.

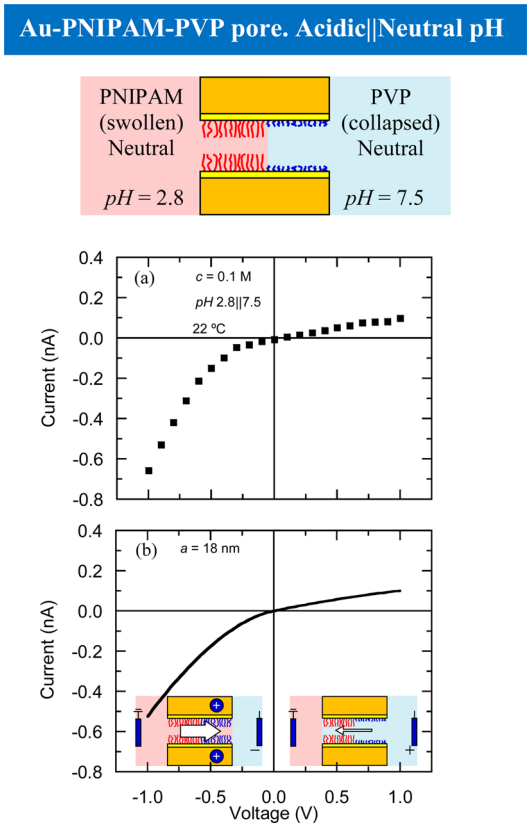

Figure 6. Experimental (a) and calculated (b) *I*–*V* curves of the Au-PNIPAM-PVP modified nanopore for the pH configuration of 2.8||7.5.

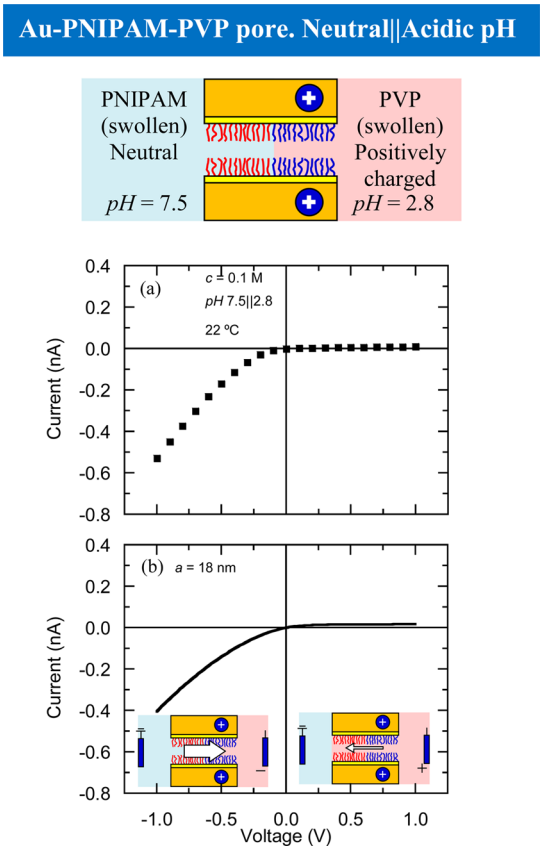

Figure 7. Experimental (a) and calculated (b) *I*–*V* curves of the Au-PNIPAM-PVP modified nanopore for the pH configuration of 7.5||2.8.

of the pore (see inset in Figure 6b). For $V > 0$, the electric field blocks the flow of H^+ ions to the pore region with uncharged PVP

dx.doi.org/10.1021/am502419j | ACS Appl. Mater. Interfaces 2014, 6, 12486−12494

chains, as in the case of pH 7.5||7.5. Figure 6b shows the theoretical results obtained using the same parameters as in the case of pH 2.8||2.8 for $V < 0$ and in the case of pH 7.5||7.5 for $V > 0$. The results are again in good agreement with the experiments, which gives support to the assumption that the H^+ ions enter or leave the entire pore solution depending on the polarity of the external voltage.

The effect of pH gradients on the ICR has been previously investigated in cylindrical nanopores,[62] conical nanopores,[63] and biological ion channels[64] with pH-sensitive fixed charges. In these cases, it was found that the pH gradient established between the two surrounding solutions gave place to non-homogeneous fixed charge distributions along the pore. As a result, the rectification ratios observed under asymmetric pH conditions were noticeably higher than those corresponding to the symmetric pH case. In our experiments, however, the rectification ratio for 0.1 M KCl solutions and $V = 1$ V decreased dramatically from $r \approx 110$ for pH 2.8||2.8 to $r \approx 7$ for pH 2.8||7.5 due to the increase of the electric current for $I > 0$ at pH values close to neutrality within the pore solution.

Figure 7 shows the results obtained with the case of pH 7.5||2.8. Now, the right side of the pore is in contact with the acidic solution, and the PVP chains are expected to be in a swollen, positively charged state. For $V > 0$, the experimental $I-V$ curves (Figure 7a) show a low conducting state practically identical to that of the case of pH 2.8||2.8. This result can be explained again assuming that the electric field drives the protons from the right solution into the pore. For $V < 0$, we observe a high conducting state, with currents lower than those found in the pH 2.8||2.8 case. The electric field removes part of the protons from the PVP region, leading to a decrease of the positive fixed charge as well as an increase of the transition region at the PNIPAM||PVP interface. Now, this decrease of the negative currents while maintaining constant the positive ones is responsible for the decrease in the rectification ratio observed in the pH 7.5||2.8 configuration. In our case, the experiments of Figure 7a give $r \approx 52$ at $V = 1$ V (less than one-half of the value $r \approx 110$ obtained in the symmetrical case of pH 2.8||2.8). The theoretical curve of Figure 7b was obtained using $\sigma_0 = 0.7\ e/\mathrm{nm}^2$, $\delta = d/6$, for $V < 0$, and the same parameters as in the case of pH 2.8||2.8 for $V > 0$. Note the good agreement between theory and experiments, showing once again that the model explains the observed experimental trends. In particlular, the theory can explain the high rectification ratios obtained, which are promising for applications concerning pH sensing and chemical actuators.

5. CONCLUSIONS

We have presented a thorough experimental and theoretical analysis of a new Au-PNIPAM-PVP modified cylindrical nanopore. Despite the approximately symmetrical pore shape, the device exhibits high rectification ratios on the order of $r = 100$ at low and intermediate electrolyte concentrations. These results were based on the ionic enrichment and depletion processes occurring at the transition zone of the non-homogeneous fixed charge distribution through the pore, which incorporates neutral and positively charged regions juxtaposed in series. The experimental characterization includes the effects of temperature, adsorption of chloride ions, electrolyte concentration, and pH of the external solutions. The results obtained were explained in terms of a theoretical continuous model providing a detailed account of the ionic concentration and electric potential axial profiles through the pore. Remarkably, the combination of well-established chemical procedures (thiol and SAM formation chemistry, electroless plating, ion-track etching) and physical models (two-region pore and Nernst−Planck equations) permits the obtainment of a highly rectifying pore, which could be scaled up to multipore membranes of potential interest for pH sensing and chemical actuators.

AUTHOR INFORMATION

Corresponding Author

*E-mail: m.ali@gsi.de or m.ali@ca.tu-darmstadt.de.

Notes

The authors declare no competing financial interest.

ACKNOWLEDGMENTS

P.R., V.G., and S.M. acknowledge the financial support from the Generalitat Valenciana (Project *PROMETEO/GV/0069*), Ministry of Science and Innovation of Spain, Materials Program (Project *MAT2012-32084*), and *FEDER*. M.A., S.N., and W.E. thank Prof. C. Trautmann and crew (GSI, Department of Materials Research) for support with irradiation experiments.

REFERENCES

(1) Siwy, Z. S. Ion-Current Rectification in Nanopores and Nanotubes with Broken Symmetry. *Adv. Funct. Mater.* **2006**, *16*, 735−746.
(2) Guo, W.; Tian, Y.; Jiang, L. Asymmetric Ion Transport through Ion-Channel-Mimetic Solid-State Nanopores. *Acc. Chem. Res.* **2013**, *46*, 2834−2846.
(3) Karnik, R.; Duan, C. H.; Castelino, K.; Daiguji, H.; Majumdar, A. Rectification of Ionic Current in a Nanofluidic Diode. *Nano Lett.* **2007**, *7*, 547−551.
(4) Zhang, Y. H.; Zhang, B.; White, H. S. Electrochemistry of Nanopore Electrodes in Low Ionic Strength Solutions. *J. Phys. Chem. B* **2006**, *110*, 1768−1774.
(5) Koo, H.-J.; Chang, S. T.; Velev, O. D. Ion-Current Diode with Aqueous Gel/SiO2 Nanofilm Interfaces. *Small* **2010**, *6*, 1393−1397.
(6) Sa, N.; Lan, W.-J.; Shi, W.; Baker, L. A. Rectification of Ion Current in Nanopipettes by External Substrates. *ACS Nano* **2013**, *7*, 11272−11282.
(7) Umehara, S.; Pourmand, N.; Webb, C. D.; Davis, R. W.; Yasuda, K.; Karhanek, M. Current Rectification with Poly-L-Lysine-Coated Quartz Nanopipettes. *Nano Lett.* **2006**, *6*, 2486−2492.
(8) Ali, M.; Ramirez, P.; Mafe, S.; Neumann, R.; Ensinger, W. A pH-Tunable Nanofluidic Diode With a Broad Range of Rectifying Properties. *ACS Nano* **2009**, *3*, 603−608.
(9) Guan, W.; Fan, R.; Reed, M. A. Field-Effect Reconfigurable Nanofluidic Ionic Diodes. *Nat. Commun.* **2011**, *2*, 506.
(10) Jiang, Y. N.; Liu, N. N.; Guo, W.; Xia, F.; Jiang, L. Highly-Efficient Gating of Solid-State Nanochannels by DNA Supersandwich Structure Containing ATP Aptamers: A Nanofluidic IMPLICATION Logic Device. *J. Am. Chem. Soc.* **2012**, *134*, 15395−15401.
(11) Mafe, S.; Manzanares, J. A.; Ramirez, P. Gating of Nanopores: Modeling and Implementation of Logic Gates. *J. Phys. Chem. C* **2010**, *114*, 21287−21290.
(12) Ramirez, P.; Ali, M.; Ensinger, W.; Mafe, S. Information Processing with a Single Multifunctional Nanofluidic Diode. *Appl. Phys. Lett.* **2012**, *101*, 133108.
(13) Ramirez, P.; Cervera, J.; Ali, M.; Ensinger, W.; Mafe, S. Logic Functions with Stimuli-Responsive Single Nanopores. *ChemElectroChem* **2014**, *1*, 698−705.
(14) Zeng, L.; Yang, Z.; Zhang, H.; Hou, X.; Tian, Y.; Yang, F.; Zhou, J.; Li, L.; Jiang, L. Tunable Ionic Transport Control inside a Bio-Inspired Constructive Bi-Channel Nanofluidic Device. *Small* **2014**, *10*, 793−801.
(15) Senapati, S.; Basuray, S.; Slouka, Z.; Cheng, L. J.; Chang, H. C.: A Nanomembrane-Based Nucleic Acid Sensing Platform for Portable Diagnostics. In *Microfluidics: Technologies and Applications;* Lin, B. C., Ed.; Topics in Current Chemistry, Springer: New York, NY, 2011; Vol. *304*; pp 153−169.

(16) Ramirez, P.; Gomez, V.; Ali, M.; Ensinger, W.; Mafe, S. Net Currents Obtained from Zero-Average Potentials in Single Amphoteric Nanopores. *Electrochem. Commun.* **2013**, *31*, 137−140.
(17) Siwy, Z.; Fulinski, A. Fabrication of a Synthetic Nanopore Ion Pump. *Phys. Rev. Lett.* **2002**, *89*, 198103.
(18) Zhang, H.; Hou, X.; Zeng, L.; Yang, F.; Li, L.; Yan, D.; Tian, Y.; Jiang, L. Bioinspired Artificial Single Ion Pump. *J. Am. Chem. Soc.* **2013**, *135*, 16102−16110.
(19) Guo, W.; Cao, L.; Xia, J.; Nie, F.-Q.; Ma, W.; Xue, J.; Song, Y.; Zhu, D.; Wang, Y.; Jiang, L. Energy Harvesting with Single-Ion-Selective Nanopores: A Concentration-Gradient-Driven Nanofluidic Power Source. *Adv. Funct. Mater.* **2010**, *20*, 1339−1344.
(20) Cervera, J.; Ramirez, P.; Mafe, S.; Stroeve, P. Asymmetric Nanopore Rectification for Ion Pumping, Electrical Power Generation, and Information Processing Applications. *Electrochim. Acta* **2011**, *56*, 4504−4511.
(21) Nasir, S.; Ramirez, P.; Ali, M.; Ahmed, I.; Fruk, L.; Mafe, S.; Ensinger, W. Nernst-Planck Model of Photo-Triggered, pH-Tunable Ionic Transport Through Nanopores Functionalized with "Caged" Lysine Chains. *J. Chem. Phys.* **2013**, *138*, 034709.
(22) Duan, R.; Xia, F.; Jiang, L. Constructing Tunable Nanopores and Their Application in Drug Delivery. *ACS Nano* **2013**, *7*, 8344−8349.
(23) Ali, M.; Nasir, S.; Ramirez, P.; Cervera, J.; Mafe, S.; Ensinger, W. Carbohydrate-Mediated Biomolecular Recognition and Gating of Synthetic Ion Channels. *J. Phys. Chem. C* **2013**, *117*, 18234−18242.
(24) Ali, M.; Neumann, R.; Ensinger, W. Sequence-Specific Recognition of DNA Oligomer Using Peptide Nucleic Acid (PNA)-Modified Synthetic Ion Channels: PNA/DNA Hybridization in Nanoconfined Environment. *ACS Nano* **2010**, *4*, 7267−7274.
(25) Ali, M.; Schiedt, B.; Neumann, R.; Ensinger, W. Biosensing with Functionalized Single Asymmetric Polymer Nanochannels. *Macromol. Biosci.* **2010**, *10*, 28−32.
(26) Ali, M.; Tahir, M. N.; Siwy, Z.; Neumann, R.; Tremel, W.; Ensinger, W. Hydrogen Peroxide Sensing with Horseradish Peroxidase-Modified Polymer Single Conical Nanochannels. *Anal. Chem.* **2011**, *83*, 1673−1680.
(27) Ali, M.; Yameen, B.; Neumann, R.; Ensinger, W.; Knoll, W.; Azzaroni, O. Biosensing and Supramolecular Bioconjugation in Single Conical Polymer Nanochannels. Facile Incorporation of Biorecognition Elements into Nanoconfined Geometries. *J. Am. Chem. Soc.* **2008**, *130*, 16351−16357.
(28) Mara, A.; Siwy, Z.; Trautmann, C.; Wan, J.; Kamme, F. An Asymmetric Polymer Nanopore for Single Molecule Detection. *Nano Lett.* **2004**, *4*, 497−501.
(29) Martin, C. R.; Siwy, Z. Molecular Filters—Pores within Pores. *Nat. Mater.* **2004**, *3*, 284−285.
(30) Tahir, M. N.; Ali, M.; Andre, R.; Muller, W. E. G.; Schroder, H.-C.; Tremel, W.; Ensinger, W. Silicatein Conjugation Inside Nanoconfined Geometries Through Immobilized NTA-Ni(II) Chelates. *Chem. Commun.* **2013**, *49*, 2210−2212.
(31) Cervera, J.; Schiedt, B.; Neumann, R.; Mafe, S.; Ramirez, P. Ionic Conduction, Rectification, and Selectivity in Single Conical Nanopores. *J. Chem. Phys.* **2006**, *124*, 104706.
(32) Constantin, D.; Siwy, Z. S. Poisson-Nernst-Planck Model of Ion Current Rectification Through a Nanofluidic Diode. *Phys. Rev. E* **2007**, *76*, 041202.
(33) Kalman, E. B.; Vlassiouk, I.; Siwy, Z. S. Nanofluidic Bipolar Transistors. *Adv. Mater.* **2008**, *20*, 293−297.
(34) Wang, X. W.; Xue, J. M.; Wang, L.; Guo, W.; Zhang, W. M.; Wang, Y. G.; Liu, Q.; Ji, H.; Ouyang, Q. Y. How the Geometric Configuration and the Surface Charge Distribution Influence the Ionic Current Rectification in Nanopores. *J. Phys. D: Appl. Phys.* **2007**, *40*, 7077−7084.
(35) Nguyen, G.; Vlassiouk, I.; Siwy, Z. S. Comparison of Bipolar and Unipolar Ionic Diodes. *Nanotechnology* **2010**, *21*, 265301.
(36) Ali, M.; Mafe, S.; Ramirez, P.; Neumann, R.; Ensinger, W. Logic Gates Using Nanofluidic Diodes Based on Conical Nanopores Functionalized with Polyprotic Acid Chains. *Langmuir* **2009**, *25*, 11993−11997.
(37) Ali, M.; Nasir, S.; Ramirez, P.; Ahmed, I.; Nguyen, Q. H.; Fruk, L.; Mafe, S.; Ensinger, W. Optical Gating of Photosensitive Synthetic Ion Channels. *Adv. Funct. Mater.* **2012**, *22*, 390−396.
(38) Hou, X.; Liu, Y. J.; Dong, H.; Yang, F.; Li, L.; Jiang, L. A pH-Gating Ionic Transport Nanodevice: Asymmetric Chemical Modification of Single Nanochannels. *Adv. Mater.* **2010**, *22*, 2440−2443.
(39) Hou, X.; Zhang, H. C.; Jiang, L. Building Bio-Inspired Artificial Functional Nanochannels: From Symmetric to Asymmetric Modification. *Angew. Chem., Int. Ed.* **2012**, *51*, 5296−5307.
(40) Vlassiouk, I.; Siwy, Z. S. Nanofluidic Diode. *Nano Lett.* **2007**, *7*, 552−556.
(41) Yameen, B.; Ali, M.; Neumann, R.; Ensinger, W.; Knoll, W.; Azzaroni, O. Single Conical Nanopores Displaying pH-Tunable Rectifying Characteristics. Manipulating Ionic Transport with Zwitterionic Polymer Brushes. *J. Am. Chem. Soc.* **2009**, *131*, 2070−2071.
(42) Kovarik, M. L.; Zhou, K.; Jacobson, S. C. Effect of Conical Nanopore Diameter on Ion Current Rectification. *J. Phys. Chem. B* **2009**, *113*, 15960−15966.
(43) Apel, P. Y.; Blonskaya, I. V.; Orelovitch, O. L.; Ramirez, P.; Sartowska, B. A. Effect of Nanopore Geometry on Ion Current Rectification. *Nanotechnology* **2011**, *22*.
(44) Ramirez, P.; Apel, P. Y.; Cervera, J.; Mafe, S. Pore Structure and Function of Synthetic Nanopores with Fixed Charges: Tip Shape and Rectification Properties. *Nanotechnology* **2008**, *19*, 315707.
(45) Ali, M.; Ramirez, P.; Nguyen, H. Q.; Nasir, S.; Cervera, J.; Mafe, S.; Ensinger, W. Single Cigar-Shaped Nanopores Functionalized with Amphoteric Amino Acid Chains: Experimental and Theoretical Characterization. *ACS Nano* **2012**, *6*, 3631−3640.
(46) Hou, X.; Yang, F.; Li, L.; Song, Y. L.; Jiang, L.; Zhu, D. B. A Biomimetic Asymmetric Responsive Single Nanochannel. *J. Am. Chem. Soc.* **2010**, *132*, 11736−11742.
(47) Ali, M.; Ramirez, P.; Nasir, S.; Nguyen, Q.-H.; Ensinger, W.; Mafe, S. Nanoparticle-Induced Rectification in a Single Cylindrical Nanopore: Net Currents From Zero Time-Average Potentials. *Appl. Phys. Lett.* **2014**, *104*, 043703.
(48) James, T.; Kalinin, Y. V.; Chan, C.-C.; Randhawa, J. S.; Gaevski, M.; Gracias, D. H. Voltage-Gated Ion Transport Through Semiconducting Conical Nanopores Formed by Metal Nanoparticle-Assisted Plasma Etching. *Nano Lett.* **2012**, *12*, 3437−3442.
(49) Muench, F.; Oezaslan, M.; Seidl, T.; Lauterbach, S.; Strasser, P.; Kleebe, H. J.; Ensinger, W. Multiple Activation of Ion Track Etched Polycarbonate for the Electroless Synthesis of Metal Nanotubes. *Appl. Phys. A: Mater. Sci. Process.* **2011**, *105*, 847−854.
(50) Muench, F.; Kunz, U.; Neetzel, C.; Lauterbach, S.; Kleebe, H.-J.; Ensinger, W. 4-(Dimethylamino)pyridine as a Powerful Auxiliary Reagent in the Electroless Synthesis of Gold Nanotubes. *Langmuir* **2010**, *27*, 430−435.
(51) Lai, J. T.; Filla, D.; Shea, R. Functional Polymers from Novel Carboxyl-Terminated Trithiocarbonates as Highly Efficient RAFT Agents. *Macromolecules* **2002**, *35*, 6754−6756.
(52) Hermann, A.; Mruk, R.; Roskamp, R. F.; Scherer, M.; Ma, L.; Zentel, R. Poly(*N*-isopropylacrylamide)-Modified Styrene-Butadiene Rubber as Thermoresponsive Material. *Macromol. Chem. Phys.* **2014**, *215*, 32−43.
(53) Hughes, C.; Yeh, L.-H.; Qian, S. Field Effect Modulation of Surface Charge Property and Electroosmotic Flow in a Nanochannel: Stern Layer Effect. *J. Phys. Chem. C* **2013**, *117*, 9322−9331.
(54) Yeh, L.-H.; Xue, S.; Joo, S. W.; Qian, S.; Hsu, J.-P. Field Effect Control of Surface Charge Property and Electroosmotic Flow in Nanofluidics. *J. Phys. Chem. C* **2012**, *116*, 4209−4216.
(55) Vlassiouk, I.; Smirnov, S.; Siwy, Z. Ionic Selectivity of Single Nanochannels. *Nano Lett.* **2008**, *8*, 1978−1984.
(56) Vlassiouk, I.; Smirnov, S.; Siwy, Z. Nanofluidic Ionic Diodes. Comparison of Analytical and Numerical Solutions. *ACS Nano* **2008**, *2*, 1589−1602.
(57) Nishizawa, M.; Menon, V. P.; Martin, C. R. Metal Nanotubule Membranes with Electrochemically Switchable Ion-Transport Selectivity. *Science* **1995**, *268*, 700−702.

(58) Shreiner, R. H.; Pratt, K. W. *Standard Reference Materials: Primary Standards and Standard Reference Materials for Electrolytic Conductivity;* U.S. Government Printing Office: Washington, DC, 2004.
(59) Ramirez, P.; Mafe, S.; Alcaraz, A.; Cervera, J. Modeling of pH-Switchable Ion Transport and Selectivity in Nanopore Membranes with Fixed Charges. *J. Phys. Chem. B* **2003**, *107*, 13178−13187.
(60) Yameen, B.; Ali, M.; Neumann, R.; Ensinger, W.; Knoll, W.; Azzaroni, O. Ionic Transport Through Single Solid-State Nanopores Controlled with Thermally Nanoactuated Macromolecular Gates. *Small* **2009**, *5*, 1287−1291.
(61) Guo, W.; Xia, H. W.; Xia, F.; Hou, X.; Cao, L. X.; Wang, L.; Xue, J. M.; Zhang, G. Z.; Song, Y. L.; Zhu, D. B.; Wang, Y. G.; Jiang, L. Current Rectification in Temperature-Responsive Single Nanopores. *ChemPhysChem* **2010**, *11*, 859−864.
(62) Fulinski, A.; Kosinska, I. D.; Siwy, Z. On the Validity of Continuous Modelling of Ion Transport Through Nanochannels. *Europhys. Lett.* **2004**, *67*, 683−689.
(63) Wang, L.; Guo, W.; Xie, Y. B.; Wang, X. W.; Xue, J. M.; Wang, Y. G. Nanofluidic Diode Generated by pH Gradient Inside Track-Etched Conical Nanopore. *Radiat. Meas.* **2009**, *44*, 1119−1122.
(64) Alcaraz, A.; Ramirez, P.; Garcia-Gimenez, E.; Lopez, M. L.; Andrio, A.; Aguilella, V. M. A pH-Tunable Nanofluidic Diode: Electrochemical Rectification in a Reconstituted Single Ion Channel. *J. Phys. Chem. B* **2006**, *110*, 21205−21209.